Extraordinary Multipole Modes and Ultra-Enhanced Optical Lateral Force by Chirality

Tongtong Zhu,[1,2] Yuzhi Shi,[3,4,*] Weiqiang Ding,[5] Din Ping Tsai,[6] Tun Cao,[1] Ai Qun Liu,[4] Manuel Nieto-Vesperinas,[7] Juan José Sáenz,[8] Pin Chieh Wu,[9] and Cheng-Wei Qiu[2,†]

[1]*School of Optoelectronic Engineering and Instrumentation Science, Dalian University of Technology, Dalian 116024, China*
[2]*Department of Electrical and Computer Engineering, National University of Singapore, Singapore 117583*
[3]*School of Mechanical Engineering, Xi'an Jiaotong University, Xi'an 710049, China*
[4]*School of Electrical and Electronic Engineering, Nanyang Technological University, Singapore 639798*
[5]*Department of Physics, Harbin Institute of Technology, Harbin 150001, China*
[6]*Department of Electronic and Information Engineering, The Hong Kong Polytechnic University, Hung Hom, Kowloon, Hong Kong, China*
[7]*Instituto de Ciencia de Materiales de Madrid, Consejo Superior de Investigaciones Científicas, Campus de Cantoblanco, Madrid 28049, Spain*
[8]*Donostia International Physics Center, 20018 Donostia-San Sebastián, Spain*
[9]*Department of Photonics, National Cheng Kung University, Tainan 70101, Taiwan*

(Received 27 February 2020; accepted 22 June 2020; published 20 July 2020)

Strong mode coupling and Fano resonances arisen from exceptional interaction between resonant modes in single nanostructures have raised much attention for their advantages in nonlinear optics, sensing, etc. Individual electromagnetic multipole modes such as quadrupoles, octupoles, and their counterparts from mode coupling (toroidal dipole and nonradiating anapole mode) have been well investigated in isolated or coupled nanostructures with access to high Q factors in bound states in the continuum. Albeit the extensive study on ordinary dielectric particles, intriguing aspects of light-matter interactions in single chiral nanostructures is lacking. Here, we unveil that extraordinary multipoles can be simultaneously superpositioned in a chiral nanocylinder, such as two toroidal dipoles with opposite moments, and electric and magnetic sextupoles. The induced optical lateral forces and their scattering cross sections can thus be either significantly enhanced in the presence of those multipoles with high-Q factors, or suppressed by the bound states in the continuum. This work for the first time reveals the complex correlation between multipolar effects, chiral coupling, and optical lateral force, providing a distinct way for advanced optical manipulation.

DOI: 10.1103/PhysRevLett.125.043901

The use of dielectric nanocavities for trapping light is of fundamental interest in physics due to the reduced dissipative loss and large resonant enhancement of both electric and magnetic fields [1–9]. Highly efficient confinement of light energy in dielectric structures is usually accompanied by the excitation of multipoles [10,11]. Examples include the electric and magnetic quadrupoles in semiconducting AlGaAs and GaAs dielectric nanoantennas [12,13], nonradiating electric toroidal and anapoles in a silicon disk [6,7,14–16], and improved second-harmonic generation efficiency in a subwavelength resonator by super cavities [8]. One viable way to realize an ideal toroidal dipole by dielectric components is to use a four-cylinder unit to excite a closed loop of magnetic field flux [14,15,17–19]. Among all the multipoles, the electric and magnetic sextupoles are rarely found.

On the other hand, with the extension of the Friedrich-Wintgen theory of bound states in the continuum (BIC) to photonics [20], there may be another mechanism to trap the light using the dielectric nanostructures. The BIC exists inside the continuum and coexists with extended waves, but they remain perfectly confined without any radiation by the interference of leaky modes [8,10,21–25]. The BIC can be found at the "crossing" of two spectral lines with different modes where the Fano resonance may collapse in a single dielectric cylinder [8–10], all-dielectric silicon metasurface [24], two interacting particles in an impurity potential [26], one-dimensional arrays [22] and two-dimensional photonic crystal slabs [20]. Although intensive studies have been done for nonchiral dielectric particles, the intriguing physics and consequences of those phenomena in a single chiral particle remain elusive and unexplored.

In this work, we, for the very first time, establish the account of realizing BICs in a chiral nanocylinder and report its complex consequences on the induced lateral optical force upon the chiral object. We demonstrate that perfect toroidal dipoles with opposite moments can be simultaneously excited in different regions of a chiral nanocylinder due to the coupling of light and the material's chirality denoted as κ [27,28]. More interesting is that other multipole modes, such as electric and magnetic sextupoles, are also found to be induced in the chiral nanocylinder,

which are rarely reported in a nonchiral single object. Those multipole modes all contribute to the enlarged scattering efficiency, resulting in the enhancement of the optical forces exerted on the chiral particle. This effect, in conjunction with the material chirality, leads to the fact that the optical force could be lateral due to the momentum transfer in the presence of chirality and more importantly such induced optical lateral force could be as strong as the optical force along the axial direction. In addition to the merit of unexplored physics, our findings make the future experimental investigation of chirality-enhanced lateral force possible. On the contrary, we could also realize BIC in the chiral nanocylinder that suppresses the scattering and optical forces consequently.

We focus on the optical lateral force (OLFs), which represents a scattered lateral electromagnetic momentum perpendicular to the incidence plane of a nongradient light beam [27–32]. Detailed derivations of the optical lateral force can be found in the Supplemental Material [33]. The lateral photon momentum can originate, e.g., from the spin-orbit coupling of a circularly polarized beam exciting surface plasmon polariton (SPP) modes [30,32,40,41], or by interference of incident, scattered, and reflected light at a dielectric surface [27]. It can also be generated from the evanescent wave excited by a circularly polarized beam [36], or in a variety of interference patterns [28,42]. On the other hand, the OLFs on a chiral nanoparticle are usually negligible due to the weak coupling of light and the particle chirality.

Here we show that the multipole dipoles can significantly enhance the OLFs up to the same order of magnitude of conventional optical radiation pressure along the light propagating (axial) direction. That is a very important step to drive the chiral particles laterally. The illustration of multipole modes in a chiral cylinder at an interface of air (refractive index $n = 1$) and water ($n = 1.337$ at the wavelength of 532 nm) is shown in Fig. 1(a). The scenario with particles at an interface holds a promising paradigm for probing optical lateral forces and sorting particles with different chiralities [38,43]. The particles are under the illumination of an obliquely incident s polarized beam with an incidence angle θ. The coupling of the chirality of the particle and the reflected and refracted light generates an optical lateral force in the y direction F_y. The mode of excitation can be flexibly tailored via the change of structural parameters like radius and length of the nanocylinder. For simplicity, we defined the size parameter $x_{\mathrm{coe}} = kr$, i.e., the product of the cylinder radius r, and the light wave number k. The aspect ratio $l_{\mathrm{coe}} = r/l$ with l being the length of the nanocylinder is also introduced.

The right images shown in Fig. 1(a) illustrate two of the excited multipole modes. In system 1 ($x_{\mathrm{coe}} = 0.982$; $l_{\mathrm{coe}} = 0.634$), two toroidal dipoles (TD) with opposite moments exist in two layers of the nanocylinder, which is optically identical to the toroidal quadrupole (TQ) [44].

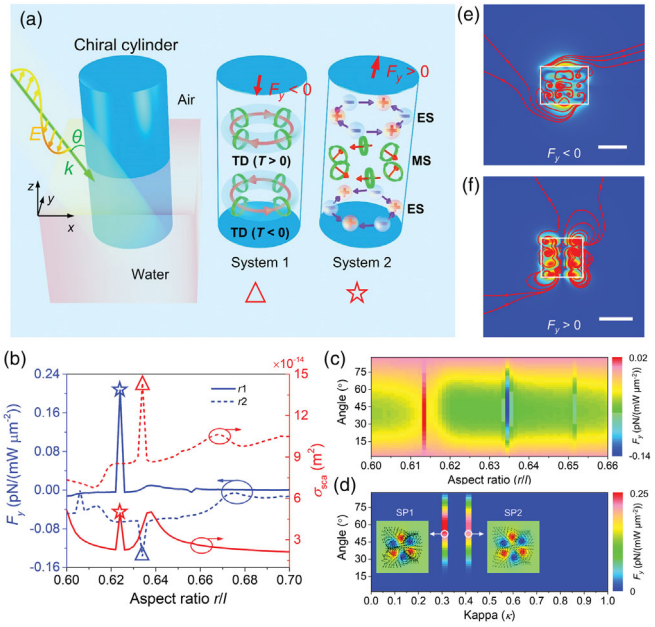

FIG. 1. Superposition of electromagnetic modes and enhanced optical lateral force from chiral nanocylinders at the water-air interface. (a) Illustration of the chiral nanocylinder under the illumination of an obliquely incident s-polarized beam with an incident angle of θ. Two multipole modes are excited when the radius and length of the cylinder change. TD: toroidal dipole. ES: electric sextupole. MS: magnetic sextupole. (b) Two TD with opposite momentums appear in the upper and lower part of the cylinder when $x_{\mathrm{coe}} = 0.982$ and $l_{\mathrm{coe}} = 0.634$ ($r1$). The cylinder has two ES on both sides and a MS in the middle when $x_{\mathrm{coe}} = 0.708$ and $l_{\mathrm{coe}} = 0.624$ ($r2$). (c) Optical lateral force with the relation of the aspect ratio and incident angle when $x_{\mathrm{coe}} = 0.982$. (d) Superpositions of ES and MS with different kappa and incident angles when $x_{\mathrm{coe}} = 0.708$ and $l_{\mathrm{coe}} = 0.624$. Sextupole (SP). The lateral force F_y is enhanced significantly in two resonance modes. Illustration of the Poynting vectors in the y-z plane indicating (e) a negative lateral force F_y in system 1 and (f) a positive F_y in system 2. Scale bars in (e) and (f) equal 100 nm.

The upper TD in the air layer has a clockwise circular magnetic field flux (see the top view of the cylinder), and an electric current surrounding the magnetic field flux, which results in a "negative toroidal moment." By contrast, the lower part of the cylinder immersed in water contains a TD with an anticlockwise circular magnetic field flux and a "positive toroidal moment."

In system 2 ($x_{\mathrm{coe}} = 0.708$; $l_{\mathrm{coe}} = 0.624$), two electric sextupoles (ES) with electric displacement currents, pointing in opposite directions, exist in the upper (air part) and lower (water part) layers of the nanocylinder. Additionally, a magnetic sextupole (MS) is excited at the middle area of the nanocylinder. It is observed that the far-field radiation pattern from a toroidal dipole is identical along an arbitrary direction in the plane of the magnetic field flux. Two isolated toroidal dipoles would produce a zero optical force everywhere on the x-y plane. Nonetheless, when one of the

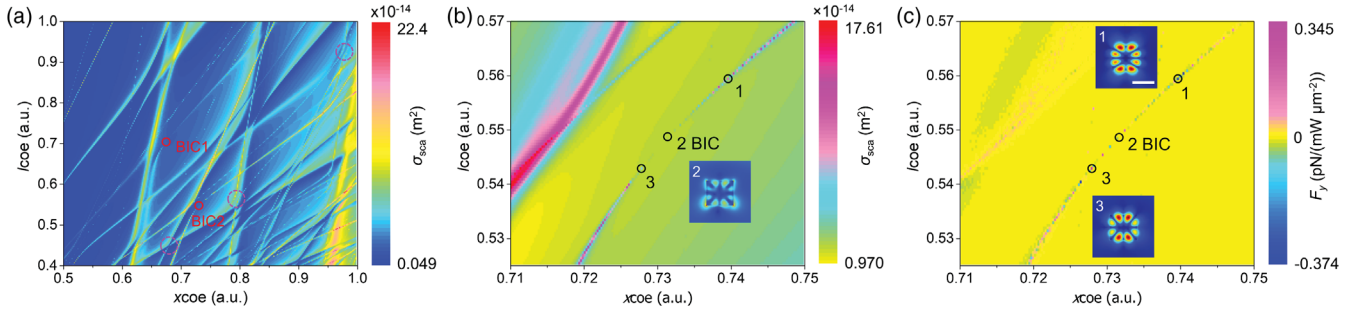

FIG. 2. Dispersion of modes and optical lateral force in a high-index chiral cylinder. (a) Scattering cross sections with dispersion modes in a high-index chiral pillar. The nanocylinder with $\varepsilon = 80$ and $\kappa = 0.4$ is under the illumination of an s-polarization beam with $\theta = 50°$. (b) Dispersion of modes near a BIC point. (c) Optical lateral forces near the BIC point. Scale bar equals 100 nm.

toroidal dipoles transits to a different dipole moment, the radiation pattern will become asymmetric, generating a negative force F_y on the cylinder in the presence of system 1. Similarly, the transition between the electric and magnetic sextupoles generates a positive component F_y when system 2 is present.

The multipole modes can be found by sweeping the aspect ratio l_{coe} as shown in Fig. 1(b). When the multipoles emerge, the spectra of the scattering cross section and the optical lateral force on the cylinder have abrupt changes. The optical resonance increases the scattering cross section in all directions. The optical lateral force can be either enhanced or suppressed according to different aspect ratios. It is shown that the incident angle has less effect on the emergence of the multipoles as shown in Figs. 1(c) and 1(d). The multipole mode is also strongly related to the aspect ratio and chirality of the nanocylinder, as shown in Figs. 1(c) and 1(d), respectively. The force F_y rises predominantly to a value comparable to that in the light propagation direction for the chirality $\kappa = 0.3$ and 0.4, where the optical scattering cross section also increases abruptly as shown in Fig. S2(b). The OLF is usually very small compared to the optical extinction force pushing nanoparticles [45,46]. When the nanocylinder presents the resonance of system 2 [SP2 in Fig. 1(c)], the OLF F_y rises prominently from near 0 to the same magnitude of F_x as shown in Fig. S2(c) of Ref. [33]. To elaborate the origin of the OLF, we plot in Figs. 1(e) and 1(f) the energy flux (Poynting vector) surrounding the nanocylinder with system 1 and 2, respectively. Three energy flux lines from the nanocylinder are scattered to the right side, while only two energy flux lines are scattered to the left side, manifesting an overall negative lateral force ($F_y < 0$) as shown in Fig. 1(e). On the contrary, more energy flux is scattered to the left side, resulting in a positive lateral force ($F_y > 0$) as shown in Fig. 1(f).

When x_{coe} and l_{coe} change, the multipole modes occur in the scattering spectrum due to the coupling of light with the

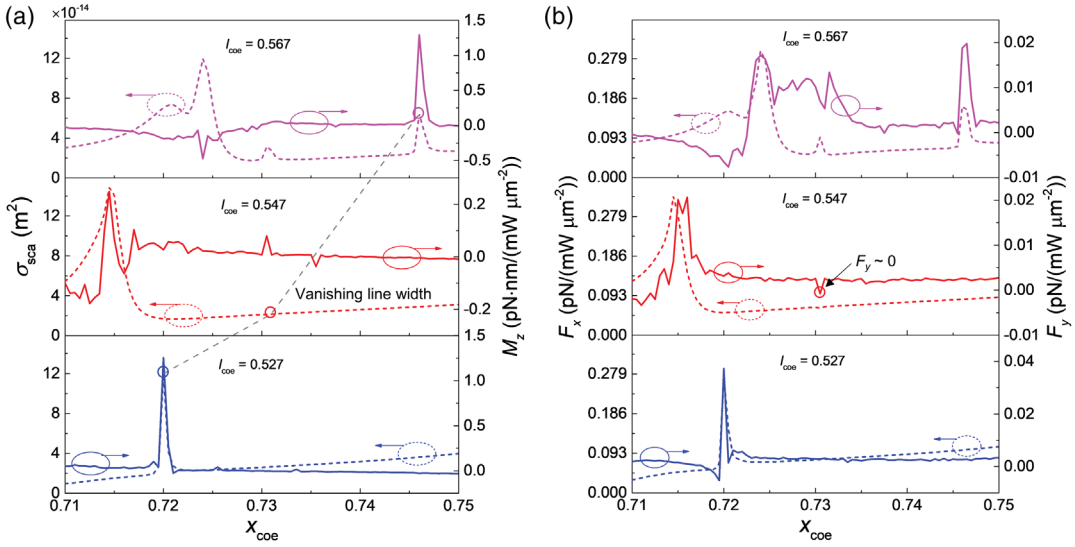

FIG. 3. Characterization of the multipole modes supported by a dielectric chiral cylinder. (a) Spectra of scattering cross section and optical torques of the chiral nanocylinders near the BIC point. The solid lines and dashed lines represent the spectra and optical torques, respectively. The ε and κ of the nanocylinder are 80 and 0.4, respectively. (b) Comparison of optical forces in the x and y directions on the nanocylinders near the BIC point.

cylinder chirality, Fabry-Pérot (FP), and Mie resonances, as shown in Fig. 2. Some of the modes intersect with each other and generate the BIC points with vanishing linewidth of the spectra, [e.g., the red solid circles in Fig. 2(a)]. The nano-cylinders trap light in the BIC points so that the scattering efficiency is mitigated, which also results in ultralow OLFs, as shown in the Supplemental Material [33]. The enlarged maps near one of the BIC points are shown in Figs. 2(b) and 2(c). The insets show the electric field of different modes in the y-z plane. The modes in points 1 (P1) and 3 (P3) are not pure TE or TM modes due to the cylinder chirality and oblique incidence of light. The point 1 contributes more to the TM mode comparing to the point 3. The BIC point (P2) has strongly trapped light on the edge of the nanocylinder. The simulation of optical forces is performed in COMSOL using Minkowski stress tensor integrated on the whole surface surrounding and with a gap of 5 nm to the nanocylinder [47,48].

Figure 3(a) depicts the scattering spectra near a BIC point ($x_{\mathrm{coe}} = 0.731$; $l_{\mathrm{coe}} = 0.547$). These spectra have sharp peaks where the multipole dipoles occur, but a vanishing line width near the BIC point. The optical torque M_z usually increases with the appearance of multipole modes with strong radiation enhancement. The component F_y in Fig. 3(b) could be enhanced to be 1 order of magnitude smaller than F_x in those multipole modes, while F_y remains to be several orders of magnitude smaller than F_x away from those multipole modes. F_y tends to be 0 at the BIC point. Interestingly, we find that F_y could reach the same order of magnitude as F_x in the presence of some particular high-order and multipole modes such as sextupole shown in Fig. 1(d).

The chirality of the nanocylinder enables the generation of circular electric currents and magnetic field flux inside the cylindrical particle, as a typical signature of toroidal modes. Figure 4 shows the distribution of displacement current density (DCD) and magnetic field flux density (MFD) inside the cylinders in system 1 and system 2. The moments of toroidal dipoles transit three times from negative to positive from $z = -20$ to 20 nm, as shown in Fig. 4(a). Interestingly, the moments of two toroidal dipoles transit between positive ($z = -20$ nm) and negative ($z = 20$ nm). They interfere and generate two magnetic dipoles (MDs) with opposite moments at $z = 0$. In another scenario, the ES transits to MS, and further to ES, from $z = -40$ to 40 nm, as shown in Fig. 4(b). Between the ES and MS, both the DCD and the MFD oscillate in six loops, generating the superposition of ES and MS at $z = -20$ and 20 nm as shown in the Supplemental Material [33]. Interestingly, and to the best of our knowledge, the ES and MS had not yet been discovered in a single dielectric element [3,49–51].

In conclusion, we have disclosed and analyzed the superposition of multipole modes and its impact upon optical lateral force in a chiral nanocylinder, under an obliquely incident polarized beam. Electric and magnetic quadrupoles, sextupoles, and toroidal dipoles, can selectively coexist at different regions of a single nanocylinder. The spectral lines of these multipole modes intersect at specific regimes as shown in the dotted circles of Fig. 2(a), and along those spectral lines, the optical lateral forces are found to be significantly enhanced. The bound states in the continuum trap the light and suppress the scattering efficiency and the optical forces. The demonstration of multipole modes and optical lateral forces on the chiral nanocylinder facilitates the development of chiral sensors and advanced optical manipulation platforms.

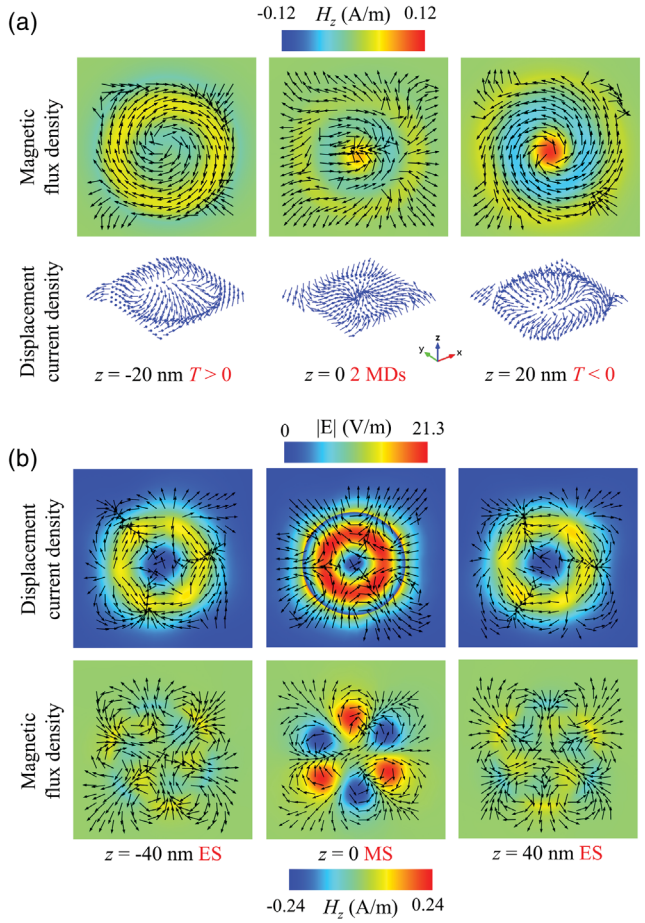

FIG. 4. Field distribution in different layers in nanocylinders in system 1 and system 2. (a) Upper row: Map of magnetic field in the z direction and arrow of magnetic flux density showing the toroidal dipole in different x-y planes with momentum T turns between $T > 0$ and $T < 0$. Lower row: Three-dimensional displacement density. And $x_{\mathrm{coe}} = 0.982$; $l_{\mathrm{coe}} = 0.634$. (b) Upper row: Map of normalized electric field and arrow of displacement current density in different x-y planes. Lower row: Map of magnetic field in the z direction and arrow of magnetic flux density. And $x_{\mathrm{coe}} = 0.708$; $l_{\mathrm{coe}} = 0.624$.

T. Z. acknowledges the Fundamental Research Funds for the Central Universities, Grant No. DUT19RC(3)046. C.-W. Q. acknowledges the financial support from the

Ministry of Education, Singapore (Project No. R-263-000-D11-114), M. N.-V. acknowledges the Spanish Ministerio de Ciencia, Innovación y Universidades, Grants No. FIS2015-69295-C3-1-P and No. PGC2018-095777-B-C21. P. C. W. acknowledges the support from Ministry of Science and Technology, Taiwan, Grants No. 108-2112-M-006-021-MY3 and No. 107-2923-M-006-004-MY3. P. C. W. also acknowledges the support in part by Higher Education Sprout Project, Ministry of Education to the Headquarters of University Advancement at National Cheng Kung University (NCKU). We thank Professor J. J. Saenz for advice.

*Corresponding author.
shiyuzhi1990@gmail.com
†Corresponding author.
eleqc@nus.edu.sg

[1] A. B. Evlyukhin, C. Reinhardt, A. Seidel, B. S. Luk'yanchuk, and B. N. Chichkov, Optical response features of Si-nanoparticle arrays, Phys. Rev. B **82**, 045404 (2010).
[2] A. García-Etxarri, R. Gómez-Medina, L. S. Froufe-Pérez, C. López, L. Chantada, F. Scheffold, J. Aizpurua, M. Nieto-Vesperinas, and J. J. Sáenz, Strong magnetic response of submicron Silicon particles in the infrared, Opt. Express **19**, 4815 (2011).
[3] A. I. Kuznetsov, A. E. Miroshnichenko, M. L. Brongersma, Y. S. Kivshar, and B. Luk'yanchuk, Optically resonant dielectric nanostructures, Science **354**, 2472 (2016).
[4] M. Decker and I. Staude, Resonant dielectric nanostructures: a low-loss platform for functional nanophotonics, J. Opt. **18**, 103001 (2016).
[5] I. Staude, T. Pertsch, and Y. S. Kivshar, All-dielectric resonant meta-optics lightens up, ACS Photonics **6**, 802 (2019).
[6] A. E. Miroshnichenko, A. B. Evlyukhin, Y. F. Yu, R. M. Bakker, A. Chipouline, A. I. Kuznetsov, B. Luk'yanchuk, B. N. Chichkov, and Y. S. Kivshar, Nonradiating anapole modes in dielectric nanoparticles, Nat. Commun. **6**, 8069 (2015).
[7] D. Smirnova and Y. S. Kivshar, Multipolar nonlinear nanophotonics, Optica **3**, 1241 (2016).
[8] K. Koshelev, S. Kruk, E. Melik-Gaykazyan, J.-H. Choi, A. Bogdanov, H.-G. Park, and Y. Kivshar, Subwavelength dielectric resonators for nonlinear nanophotonics, Science **367**, 288 (2020).
[9] W. Chen, Y. Chen, and W. Liu, Multipolar conversion induced subwavelength high-Q Kerker supermodes with unidirectional radiations, Laser Photonics Rev. **13**, 1900067 (2019).
[10] M. V. Rybin, K. L. Koshelev, Z. F. Sadrieva, K. B. Samusev, A. A. Bogdanov, M. F. Limonov, and Y. S. Kivshar, High-Q Supercavity Modes in Subwavelength Dielectric Resonators, Phys. Rev. Lett. **119**, 243901 (2017).
[11] I. Staude *et al.*, Tailoring directional scattering through magnetic and electric resonances in subwavelength silicon nanodisks, ACS Nano **7**, 7824 (2013).
[12] L. Carletti, A. Locatelli, D. Neshev, and C. De Angelis, Shaping the radiation pattern of second-harmonic generation from AlGaAs dielectric nanoantennas, ACS Photonics **3**, 1500 (2016).
[13] J. D. Sautter *et al.*, Tailoring second-harmonic emission from (111)-GaAs nanoantennas, Nano Lett. **19**, 3905 (2019).
[14] A. A. Basharin, M. Kafesaki, E. N. Economou, C. M. Soukoulis, V. A. Fedotov, V. Savinov, and N. I. Zheludev, Dielectric Metamaterials with Toroidal Dipolar Response, Phys. Rev. X **5**, 011036 (2015).
[15] D. A. Smirnova, A. B. Khanikaev, L. A. Smirnov, and Y. S. Kivshar, Multipolar third-harmonic generation driven by optically induced magnetic resonances, ACS Photonics **3**, 1468 (2016).
[16] W. Liu, J. Zhang, and A. E. Miroshnichenko, Toroidal dipole-induced transparency in core–shell nanoparticles, Laser Photonics Rev. **9**, 564 (2015).
[17] V. R. Tuz, V. V. Khardikov, and Y. S. Kivshar, All-dielectric resonant metasurfaces with a strong toroidal response, ACS Photonics **5**, 1871 (2018).
[18] V. Savinov, N. Papasimakis, D. P. Tsai, and N. I. Zheludev, Optical anapoles, Commun. Phys. **2**, 69 (2019).
[19] P. C. Wu *et al.*, Optical anapole metamaterial, ACS Nano **12**, 1920 (2018).
[20] C. W. Hsu, B. Zhen, J. Lee, S.-L. Chua, S. G. Johnson, J. D. Joannopoulos, and M. Soljačić, Observation of trapped light within the radiation continuum, Nature (London) **499**, 188 (2013).
[21] C. W. Hsu, B. Zhen, A. D. Stone, J. D. Joannopoulos, and M. Soljačić, Bound states in the continuum, Nat. Rev. Mater. **1**, 16048 (2016).
[22] D. C. Marinica, A. G. Borisov, and S. V. Shabanov, Bound States in the Continuum in Photonics, Phys. Rev. Lett. **100**, 183902 (2008).
[23] A. A. Bogdanov, K. L. Koshelev, P. V. Kapitanova, M. V. Rybin, S. A. Gladyshev, Z. F. Sadrieva, K. B. Samusev, Y. S. Kivshar, and M. F. Limonov, Bound states in the continuum and Fano resonances in the strong mode coupling regime, Adv. Photon. **1**, 016001 (2019).
[24] S. Han *et al.*, All-dielectric active terahertz photonics driven by bound states in the continuum, Adv. Mater. **31**, 1901921 (2019).
[25] G. Li, S. Zhang, and T. Zentgraf, Nonlinear photonic metasurfaces, Nat. Rev. Mater. **2**, 17010 (2017).
[26] J. M. Zhang, D. Braak, and M. Kollar, Bound States in the Continuum Realized in the One-Dimensional Two-Particle Hubbard Model with an Impurity, Phys. Rev. Lett. **109**, 116405 (2012).
[27] S. B. Wang and C. T. Chan, Lateral optical force on chiral particles near a surface, Nat. Commun. **5**, 3307 (2014).
[28] T. Zhang, M. R. C. Mahdy, Y. Liu, J. H. Teng, C. T. Lim, Z. Wang, and C.-W. Qiu, All-optical chirality-sensitive sorting via reversible lateral forces in interference fields, ACS Nano **11**, 4292 (2017).
[29] A. Hayat, J. P. B. Mueller, and F. Capasso, Lateral chirality-sorting optical forces, Proc. Natl. Acad. Sci. U.S.A. **112**, 13190 (2015).

[30] F. J. Rodríguez-Fortuño, N. Engheta, A. Martínez, and A. V. Zayats, Lateral forces on circularly polarizable particles near a surface, Nat. Commun. **6**, 8799 (2015).
[31] H. Magallanes and E. Brasselet, Macroscopic direct observation of optical spin-dependent lateral forces and left-handed torques, Nat. Photonics **12**, 461 (2018).
[32] D. O'Connor, P. Ginzburg, F. J. Rodríguez-Fortuño, G. A. Wurtz, and A. V. Zayats, Spin-orbit coupling in surface plasmon scattering by nanostructures, Nat. Commun. **5**, 5327 (2014).
[33] See Supplemental Material at http://link.aps.org/supplemental/10.1103/PhysRevLett.125.043901 for the detailed derivation of the lateral force by chirality and Figs. S1-S7, which includes Refs. [27,28,34–39].
[34] M. Nieto-Vesperinas, J. J. Sáenz, R. Gómez-Medina, and L. Chantada, Optical forces on small magnetodielectric particles, Opt. Express **18**, 11428 (2010).
[35] R. Gómez-Medina, M. Nieto-Vesperinas, and J. J. Sáenz, Nonconservative electric and magnetic optical forces on submicron dielectric particles, Phys. Rev. A **83**, 033825 (2011).
[36] K. Y. Bliokh, A. Y. Bekshaev, and F. Nori, Extraordinary momentum and spin in evanescent waves, Nat. Commun. **5**, 3300 (2014).
[37] C. F. Bohren and D. R. Huffman, *Absorption and Scattering of Light by Small Particles* (John Wiley & Sons, New York, 2008).
[38] S. Sukhov, V. Kajorndejnukul, R. R. Naraghi, and A. Dogariu, Dynamic consequences of optical spin-orbit interaction, Nat. Photonics **9**, 809 (2015).
[39] L. Novotny and B. Hecht, *Principles of Nano-Optics* (Cambridge University Press, Cambridge, England, 2012).
[40] Q. Zhang, J. Li, and X. Liu, Optical lateral forces and torques induced by chiral surface-plasmon-polaritons and their potential applications in recognition and separation of chiral enantiomers, Phys. Chem. Chem. Phys. **21**, 1308 (2019).
[41] M. H. Alizadeh and B. M. Reinhard, Transverse Chiral Optical Forces by Chiral Surface Plasmon Polaritons, ACS Photonics **2**, 1780 (2015).
[42] H. Chen, C. Liang, S. Liu, and Z. Lin, Chirality sorting using two-wave-interference–induced lateral optical force, Phys. Rev. A **93**, 053833 (2016).
[43] V. Kajorndejnukul, W. Ding, S. Sukhov, C.-W. Qiu, and A. Dogariu, Linear momentum increase and negative optical forces at dielectric interface, Nat. Photonics **7**, 787 (2013).
[44] V. Savinov, V. A. Fedotov, and N. I. Zheludev, Toroidal dipolar excitation and macroscopic electromagnetic properties of metamaterials, Phys. Rev. B **89**, 205112 (2014).
[45] Y. Z. Shi *et al.*, Sculpting nanoparticle dynamics for single-bacteria-level screening and direct binding-efficiency measurement, Nat. Commun. **9**, 815 (2018).
[46] Y. Shi *et al.*, Nanometer-precision linear sorting with synchronized optofluidic dual barriers, Sci. Adv. **4**, eaao0773 (2018).
[47] Y. Shi *et al.*, Nanophotonic array-induced dynamic behavior for label-free shape-selective bacteria sieving, ACS Nano **13**, 12070 (2019).
[48] Y. Z. Shi *et al.*, High-resolution and multi-range particle separation by microscopic vibration in an optofluidic chip, Lab Chip **17**, 2443 (2017).
[49] Y. Kivshar, All-dielectric meta-optics and non-linear nanophotonics, Natl. Sci. Rev. **5**, 144 (2018).
[50] Y. Yang, A. E. Miroshnichenko, S. V. Kostinski, M. Odit, P. Kapitanova, M. Qiu, and Y. S. Kivshar, Multimode directionality in all-dielectric metasurfaces, Phys. Rev. B **95**, 165426 (2017).
[51] W. Liu and Y. S. Kivshar, Multipolar interference effects in nanophotonics, Phil. Trans. R. Soc. A **375**, 20160317 (2017).